DELPHI Collaboration

DELPHI 2001-022 CONF 463
7 March, 2001

Results on Fermion-Pair Production at LEP running in 2000

A.Behrmann[1], I.Boyko[2], P.Checchia[3], G.Della Ricca[4], I.Gouz[5], J.Holt[6], M.Nikolenko[2], A.Olchevski[2], M.Paganoni[3], D.Reid[7], P.Renton[6], G.Morton[6], T.Myklebust[8], G.R.Wilkinson[6], M.Winter[9], V.Zhuravlov[2]

Abstract

A preliminary analysis of the data collected in 2000 with the DELPHI detector at e^+e^- collision energy above 200 GeV was performed in order to extract the hadronic and leptonic cross-sections, as well as the leptonic forward-backward asymmetries. Various interpretations of the results, including possible physics beyond the Standard Model, are presented. In particular, the data are used to investigate potential contact interactions and for Z' bosons.

Results prepared for Winter Conferences 2001

[1]Fachbereich Physik, University of Wuppertal, Wuppertal, FRG
[2]Joint Institute for Nuclear Research, Dubna, Russia
[3]INFN, Padova, Italy
[4]INFN, Trieste, Italy
[5]INFN, Milano, Italy
[6]Department of Physics, University of Oxford, Oxford,UK
[7]NIKHEF, Postbus 41882, NL-1009 DB Amsterdam, The Netherlands
[8]University of Oslo, Institute of Physics, Oslo, Norway
[9]Institut de Recherches Subatomiques, IN2P3-CNRS/ULP, Strasbourg, France

1 Introduction

Preliminary results are presented from the analyses of fermion-pair final states collected in 2000 with the DELPHI experiment [1] at centre-of-mass energies, $\sqrt{s}$, above 200 GeV. Measurements of cross-sections for inclusive hadronic, electron-positron pairs, muon-pair and tau-pair final states are given, together with leptonic forward-backward asymmetries. These results complement those obtained from data collected from 1995 to 1999 at lower collision energies from 130 to 202 GeV [2, 3, 4]. Polar angle distributions of $\mu^+\mu^-$ and $\tau^+\tau^-$ events are also given, adding to the results provided in [3, 4].

The measurements of the cross-sections and forward-backward asymmetries together with the results presented in [2, 3, 4] and from LEP running in the vicinity of the Z-resonance [5, 6], are used to update the searches for new physics involving contact interactions and additional neutral gauge bosons, given in [2, 3, 4]. For the theoretical motivation and technical details, the reader is referred to [2, 3, 4].

Results on fermion-pair production at LEP at collision energies from 130 to 202 GeV from the other LEP collaborations can be found in [7], together with limits derived from these results.

The measurements of cross-sections, forward-backward asymmetries and angular distributions are given in section 2. The interpretations of the data are presented in section 3. A summary and conclusions are provided in section 4.

2 Measurements of cross-sections and asymmetries

2.1 Luminosity and centre-of-mass energy

The luminosity analysis of the data collected during LEP operation in 2000 followed closely the one described in [2, 3]. The total experimental systematic uncertainty on the integrated luminosity determination amounts to 1.00%, to be combined with a 0.25% uncertainty reflecting the precision of the theoretical calculations underlying the computation of the cross-section visible in the luminometers. The errors are to be added in quadrature to the other sources of systematics uncertainty given below.

In previous years there has either been one distinct mean collision energy or several well separated mean collision energies for the data analysed. In 2000 the luminosity has been delivered in a distribution which is approximately a continuum. Although there are some clear peaks in the distribution of luminosity as a function of mean collision energy, the points at which to divide the data into different bins are somewhat arbitrary.

Except for electron-positron final states, the data has been divided into two ranges of collision energies for analysis: from 202.5 to 205.5 GeV and above 205.5 GeV. In this paper these are referred to as being at energies of approximately 205 and 206 GeV respectively. Figure 1 shows the distribution of luminosity as a function of centre-of-mass energy. The luminosities used for the analysis of the inclusive hadronic final states and estimates of the mean centre-of-mass energy [8] are given in Table 1. The centre-of-mass energies for each of the analyses were determined from preliminary online estimates of the LEP collision energy. These are accurate to 200 MeV.

2.2 Measurements

As in [2, 3, 4], the cross-sections and asymmetry measurements are given for different ranges of the reduced centre-of-mass energy, $\sqrt{s'}$: for hadronic final states an *inclusive* sample, defined as $\sqrt{s'}/\sqrt{s} > 0.10$, and a *non-radiative* sample, defined as $\sqrt{s'}/\sqrt{s} > 0.85$; for muon and tau final states an *inclusive* sample with $\sqrt{s'} > 75\,\mathrm{GeV}$, and a *non-radiative* sample with $\sqrt{s'}/\sqrt{s} > 0.85$. For electron-positron final states, a cut on the acollinearity[1] angle between the electron and positron, $\theta_{acol} < 20^\circ$, was applied, corresponding approximately to a cut of $\sqrt{s'}/\sqrt{s} > 0.85$. The number of events selected for each final state are given in Table 2.

The results on the cross-section and leptonic forward-backward asymmetry measurements presented in this section are from the analyses of e^+e^-, $\mu^+\mu^-$, $\tau^+\tau^-$ and inclusive hadronic final states. These analyses were similar to the ones performed at lower energies and the details, such as event selection and reduced energy determination can be found, in [2, 3, 4].

The distributions of $\sqrt{s'}/\sqrt{s}$ obtained for the real and the simulated data are shown in Figure 2 for the hadronic channel and Figure 3 for the muon and tau channels. The methods of estimating $\sqrt{s'}$ correspond to slightly different definitions of this variable. For $\mu^+\mu^-$ and the $\tau^+\tau^-$ final states, $\sqrt{s'}$ is the invariant mass of the muons or tau-leptons in the final state. For the inclusive hadronic final states, the estimated $\sqrt{s'}$ can be considered in theoretical predictions to be the invariant mass of the s-channel propagator.

For the $\mu^+\mu^-$ and $\tau^+\tau^-$ final states, the cross-sections and asymmetries were extrapolated to 4π acceptance using samples of events generated with KORALZ [13]. The calculations of KORALZ do not account for interference between Initial State and Final State Radiation. Corrections to the extrapolation for this interference were determined using the semi-analytical calculations of ZFITTER [14], in which the interference was computed to $\mathcal{O}(\alpha)$, and applied to the results. To account for missing higher order corrections, a systematic uncertainty of half the correction was taken. For the inclusive hadronic states, any correction for the interference between initial and final state radiation was estimated to be negligibly small within the precision of the measurement.

2.3 Failure of part of the DELPHI TPC

During the operation of the DELPHI detector in 2000 one of the 12 sectors of the central tracking chamber, the TPC [1], failed. After the 1$^{\mathrm{st}}$ of September it was not possible to detect the tracks left by charged particles inside the broken sector. Never the less, the redundancy of the tracking system of DELPHI meant that tracks passing through the sector could still be reconstructed from signal in any of the other tracking detectors. The tracks reconstruction efficicency was slightly reduced in the region covered by the broken sector, and on average the resolution on the perigee parameters of the tracks was worse than in prior to the failure of the sector. To allow studies of the data taken after the 1$^{\mathrm{st}}$ of September samples of events have been simulated dropping information from the broken sector of the TPC. The failure of the TPC had a different impact on the analyses of each of the final states.

For electron-positron final states the impact was negligible. The energy measurements

[1] The acollinearity angle between two particles is defined as $\cos\theta_{acol} = -p_1.p_2/|p_1||p_2|$, where p_1 and p_2 are the 3-momenta of the particles.

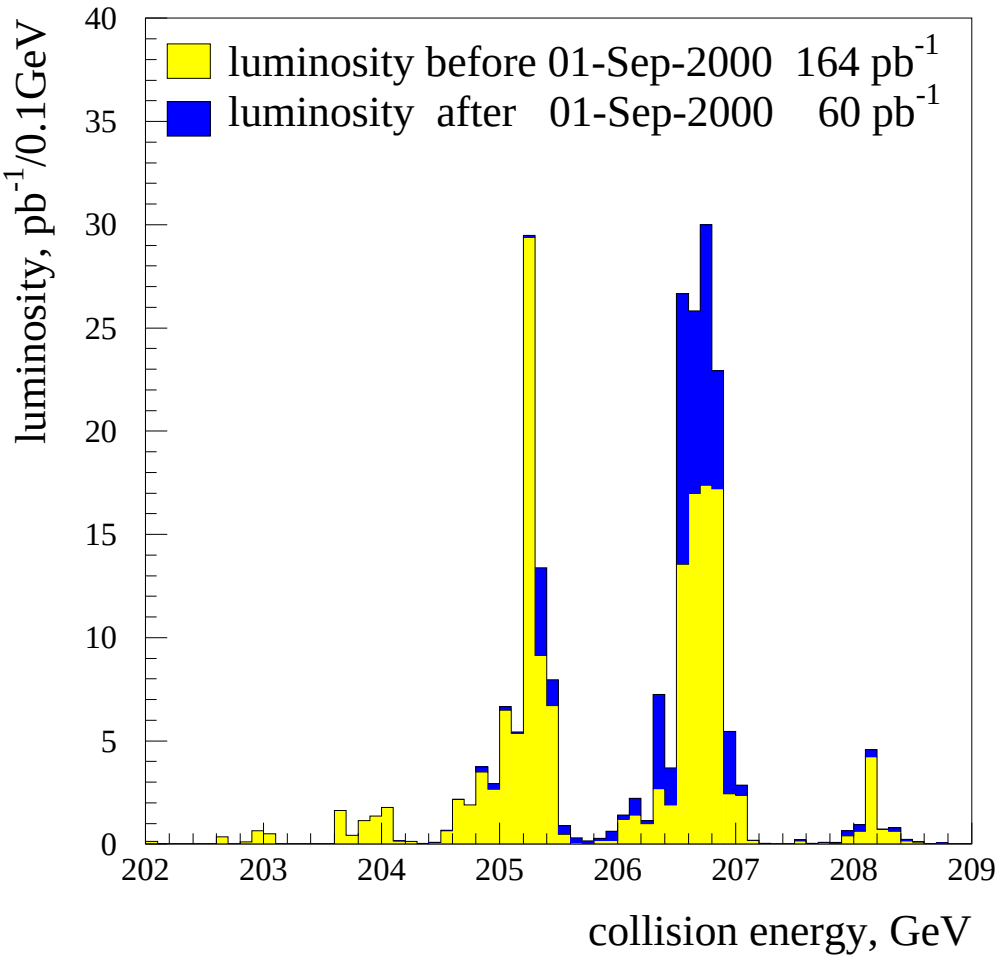

Figure 1: The distribution of luminosity as a function of energy. The luminosity is separated into that taken before and after the 1st of September. The luminosity collected in the latter period was taken with one sector of the TPC broken.

Channel	Nominal Energy (GeV)	Mean Energy (GeV)	Luminosity (pb^{-1})
$e^+e^- \to q\bar{q}(\gamma)$	205	205.0	75.0
	206	206.8	85.4
$e^+e^- \to e^+e^-(\gamma)$	205	205.4	160.0
	206	206.5	51.5
$e^+e^- \to \mu^+\mu^-(\gamma)$	205	205.0	82.5
	206	206.7	139.8
$e^+e^- \to \tau^+\tau^-(\gamma)$	205	205.1	83.4
	206	206.7	138.4

Table 1: The luminosities and collision energies for different final states. The large differences between channels are caused by the failure of part of the TPC and the different division of data into high and low energy points for the electron-positron data.

Channel	Collision Energy (GeV)	
	~ 205	~ 206
$e^+e^- \to q\bar{q}(\gamma)$	6292	7017
$e^+e^- \to e^+e^-(\gamma)$	2702	935
$e^+e^- \to \mu^+\mu^-(\gamma)$	393	634
$e^+e^- \to \tau^+\tau^-(\gamma)$	252	373

Table 2: The statistics used in the analyses of the different final states. For each channel, the values refer to the samples with $\sqrt{s'/s} > 0.10$ for hadrons, $\sqrt{s'} > 75$ for muons and taus and $\theta_{acol} < 20^\circ$ for electron-positron pairs.

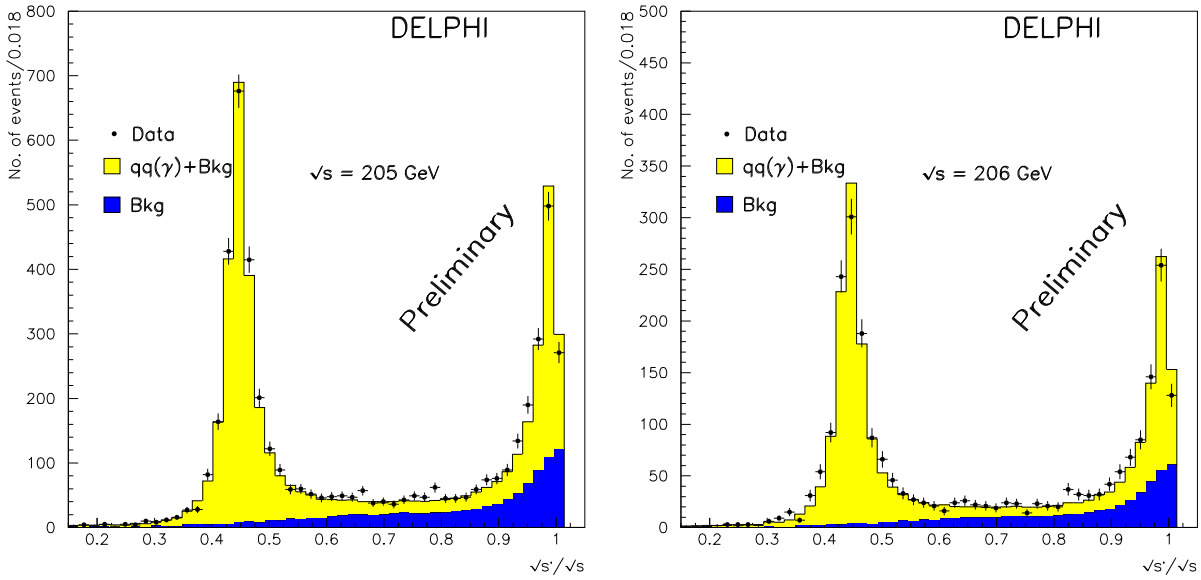

Figure 2: Distributions of the reconstructed reduced energy for the $e^+e^- \to q\bar{q}(\gamma)$ process at $\sqrt{s} \sim 205$ and 206 GeV. The points show the real data, and the histograms show the simulated signal and background samples. The expected signals are simulated with the PYTHIA [9] generator and are normalised to the luminosities of the data set analysed. Differences between data and simulation in the shape of these distributions are taken into account when determining the systematic errors on the measured cross-sections.

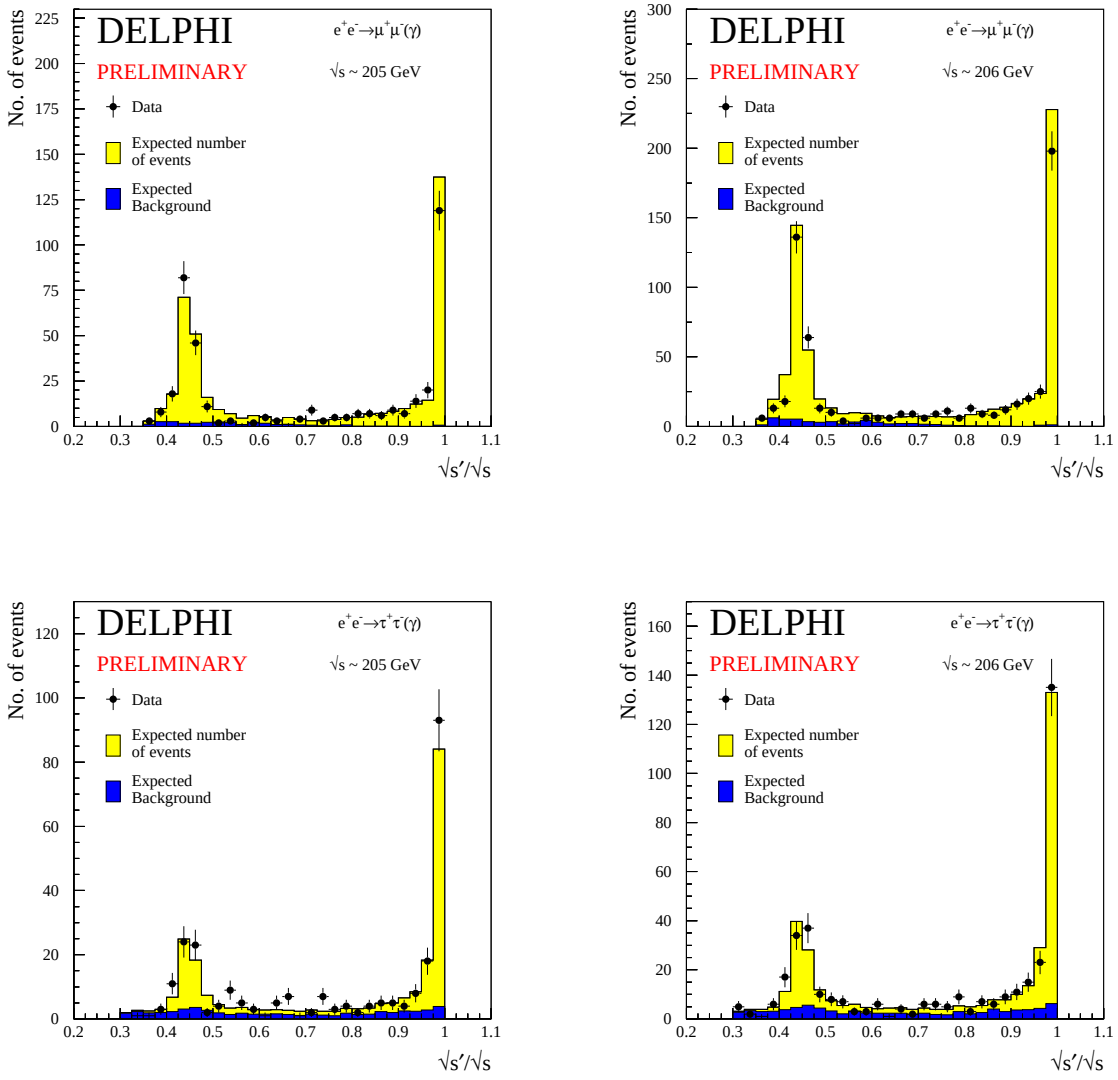

Figure 3: Distributions of the reconstructed reduced energy for the $e^+e^- \to \mu^+\mu^-(\gamma)$ and $e^+e^- \to \tau^+\tau^-(\gamma)$ processes at $\sqrt{s} \sim 205$ and 206 GeV. The points stand for the data and the histograms represent the signal and background. The expected signals are simulated with the KORALZ [13] generator scaled to the ZFITTER [14] predictions and are normalised to the luminosities of the data sets analysed.

in the electromagnetic calorimeters being more important. Results are given for the two periods separately. All data taken up to the 1st of September and data taken after that date have mean centre-of-mass energies of 205.4 GeV and 206.5 GeV respectively. These are referred to as being at energies of approximately 205 and 206 GeV.

For the muon-pair analysis, it was decided to exclude events containing any track in the broken sector of the TPC, so that the worse momentum resolution for tracks in the TPC did not adversely effect the analysis. Similarly, for the tau-pair analysis, events were rejected if the leading track of one hemisphere of the event was in the broken sector. For both these final states, a cut on the direction of tracks in the detector is a good aproximation to a cut on the direction of the fermions. Since there are two fermions per events, the cut applied reduces the efficiency of the analyses by approximately 1/6 for the data taken with the broken TPC sector. The cross-section results in the two periods have been averaged together using a weighted average taking into account the correlations between the systematic errors in the two periods. The forward-backward asymmetries have been computed by adding together the numbers of signal events in each period.

For hadronic final states the width of the jets in the detector means that even though the direction of the produced quarks may not point towards the broken sector of the TPC, particles may still pass through the sector. The effect of this on the analysis is non-trivial to estimate. For the results presented here only data taken up to the 1st of September were used. Hence the lower luminosity given in Table 1 for the hadronic final states compared to the leptonic final states.

Further studies of the data taken after the 1st of September are in progress. The intention is to be able to use all the available data for the final analyses.

2.4 Results

Figures 4 shows the measured hadron, electron-positron pair, muon-pair and tau-pair cross-sections from DELPHI for all collision energies ranging from 130 up to 206 GeV. The forward-backward asymmetries for electron-positron pairs, muon-pairs and tau-pairs are shown in Figure 5. The Standard Model (SM) predictions are from the TOPAZ0 program [15] for electron-positron final states and the ZFITTER program [14] for the others.

Statistical uncertainties and systematic errors due to the event selection and to the residual background subtraction are shown in Table 3. For the cross-section measurements, they are to be added in quadrature to the uncertainty coming from the luminosity determination. The uncertainties on the theoretical predictions for the s-channels $e^+e^-\to\mu^+\mu^-$, $e^+e^-\to\tau^+\tau^-$ and inclusive hadronic cross-sections are estimated to be below 1%.

In addition to the measurements of the cross-sections and asymmetries, measurements of the differential cross-sections, $d\sigma/d\cos\theta$, are measured for the $\mu^+\mu^-$ and $\tau^+\tau^-$ final states for the *non-radiative* samples. For the $\mu^+\mu^-$ final states, the scattering angle θ is the angle of the negative fermion with respect to the incoming electron in the laboratory frame. For the $\tau^+\tau^-$ final states, the angle is defined as in [3]. The weighted average of the differential cross-sections for $\sqrt{s}\sim 205-206\,\mathrm{GeV}$ for $\mu^+\mu^-$ and $\tau^+\tau^-$ final states are shown in Figure 6. The Standard Model expectations evaluated with ZFITTER at the average centre-of-mass energy are shown for comparison.

Overall, no substantial departure of the measurements from the Standard Model predictions was found.

3 Fits to physics beyond the Standard Model

The data presented in this paper were used to improve the constraints on physics beyond the Standard Model given in [2, 3, 4] for two sets of models: contact interactions between leptons and models including additional, neutrl gauge bosons, Z′. The theoretical bases of each of these models are discussed in section 5 of [2], the key points are summarised below. Unless otherwise stated, systematic errors for LEP II measurements were added in quadrature with the statistical errors and treated as uncorrelated between measurements.

3.1 Contact interaction models

The parameter fitted was $\epsilon = 1/\Lambda^2$, where Λ is the scale of the interactions in the effective Lagrangian of the four-fermion interactions:

$$\mathcal{L}_{eff} = \frac{g^2}{(1+\delta)\Lambda^2} \sum_{i,j=L,R} \eta_{ij} \overline{e}_i \gamma_\mu e_i \overline{f}_j \gamma^\mu f_j. \quad (1)$$

where the i, j denote either left or right handed helicities of the fermionic currents involved. Different choices of η_{ij} lead to 12 commonly studied models, referred to as LL, RR etc [16]. See sections 5.1 and 6.1.1 of [2] for more details.

A fit for contact interactions between leptons ($e^+e^- \to l^+l^-$), assuming lepton universality in the couplings, was made using data from $e^+e^- \to e^+e^-, e^+e^- \to \mu^+\mu^-$ and $e^+e^- \to \tau^+\tau^-$ at all energies from 130 to 202 GeV. The values of ϵ extracted for each model were all compatible with the Standard Model expectation, $\epsilon = 0$, at the two standard deviation level. The errors on ϵ are typically 10% smaller than those reported in [4] as a result of the inclusion of the new data. The fitted values of ϵ were converted into lower limits on Λ at 95% confidence level, as in [2]. The results are given in Table 4 and shown graphically in Figure 7.

3.2 Z′-bosons

Existing data from LEP1 and LEP2 and the cross-sections and asymmetries given here were used to fit the data to models including additional neutral gauge bosons, Z′.

3.2.1 Model dependent fits

Fits were made to the mass of a Z′, $M_{Z'}$, the mass of the Z, M_Z, and to the mixing angle between the two bosonic fields, $\Theta_{ZZ'}$, for 4 different models referred to as χ, ψ, η and L-R [17]. More details can be found in section 5.4.1 and 6.3.1 of [2]. The fitted value of M_Z was found to be in agreement with the value found from fits to the data with no Z′. No evidence was found for the existence of a Z′-boson in any of the models. The 95 % confidence level limits on $M_{Z'}$ and $\Theta_{ZZ'}$ were computed for the different models by determining the contours of the domain in the $M_{Z'} - \Theta_{ZZ'}$ plane where $\chi^2 < \chi^2_{min} + 5.99$ [18]. The allowed regions for $M_{Z'}$ and $\Theta_{ZZ'}$ are shown in Figure 8. The lower limits, shown in

Non-radiative								
$\sqrt{s}$		$\Delta\sigma^h/\sigma^h$	$\Delta\sigma^e/\sigma^e$	$\Delta\sigma^\mu/\sigma^\mu$	$\Delta\sigma^\tau/\sigma^\tau$	$\Delta A_{FB}{}^e$	$\Delta A_{FB}{}^\mu$	$\Delta A_{FB}{}^\tau$
GeV		%	%	%	%	10^{-3}	10^{-3}	10^{-3}
~ 205	(stat.)	3.3	2.4	7.8	10.4	11	60	81
	(syst.)	2.6	1.0	3.3	3.3	$^{+10}_{-3}$	1	15
~ 206	(stat.)	3.2	3.2	7.4	8.3	19	49	66
	(syst.)	2.6	0.9	3.1	3.6	$^{+10}_{-3}$	1	15

Inclusive								
$\sqrt{s}$		$\Delta\sigma^h/\sigma^h$	$\Delta\sigma^e/\sigma^e$	$\Delta\sigma^\mu/\sigma^\mu$	$\Delta\sigma^\tau/\sigma^\tau$	$\Delta A_{FB}{}^e$	$\Delta A_{FB}{}^\mu$	$\Delta A_{FB}{}^\tau$
GeV		%	%	%	%	10^{-3}	10^{-3}	10^{-3}
~ 205	(stat.)	1.6	–	5.1	7.9	–	48	78
	(syst.)	1.8	–	3.4	4.2	–	2	15
~ 206	(stat.)	1.5	–	4.0	6.6	–	37	66
	(syst.)	1.9	–	3.6	4.2	–	2	15

Table 3: Statistical and systematic uncertainties of the *non-radiative* and *inclusive* cross section and forward-backward asymmetry measurements for the different final states. *Non-radiative* refers to $\sqrt{s'}/\sqrt{s} > 0.85$ for muon, tau and hadronic final states, and $\theta_{acol} < 20^\circ$ for electron-positron pairs. *Inclusive* refers to $\sqrt{s'}/\sqrt{s} > 0.10$ for the hadronic final states and to $\sqrt{s'} > 75$ GeV for the muon and tau final states. The luminosity uncertainties (1.00% experimental and 0.25% theoretical) are not included.

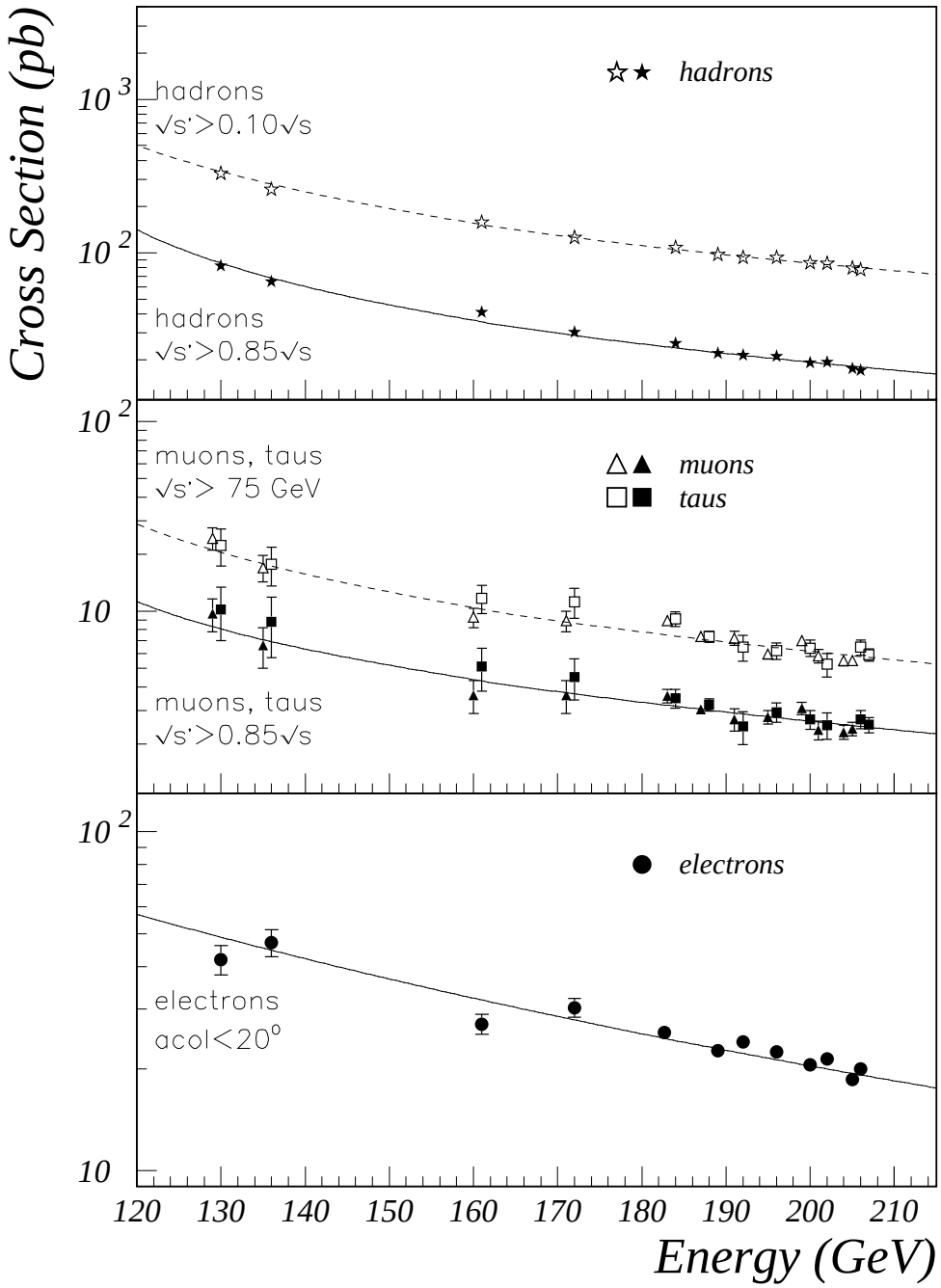

Figure 4: cross-sections for the $e^+e^- \to q\bar{q}(\gamma)$, $\mu^+\mu^-(\gamma)$ and $\tau^+\tau^-(\gamma)$, and $e^+e^- \to e^+e^-(\gamma)$ processes measured at energies from 130 up to 206 GeV. The curves show the SM prediction of the TOPAZ0 program [15] for electron-positron final states and the ZFITTER program [14] for the other final states. Open points represent the *inclusive* selections and solid points the *non-radiative* selections.

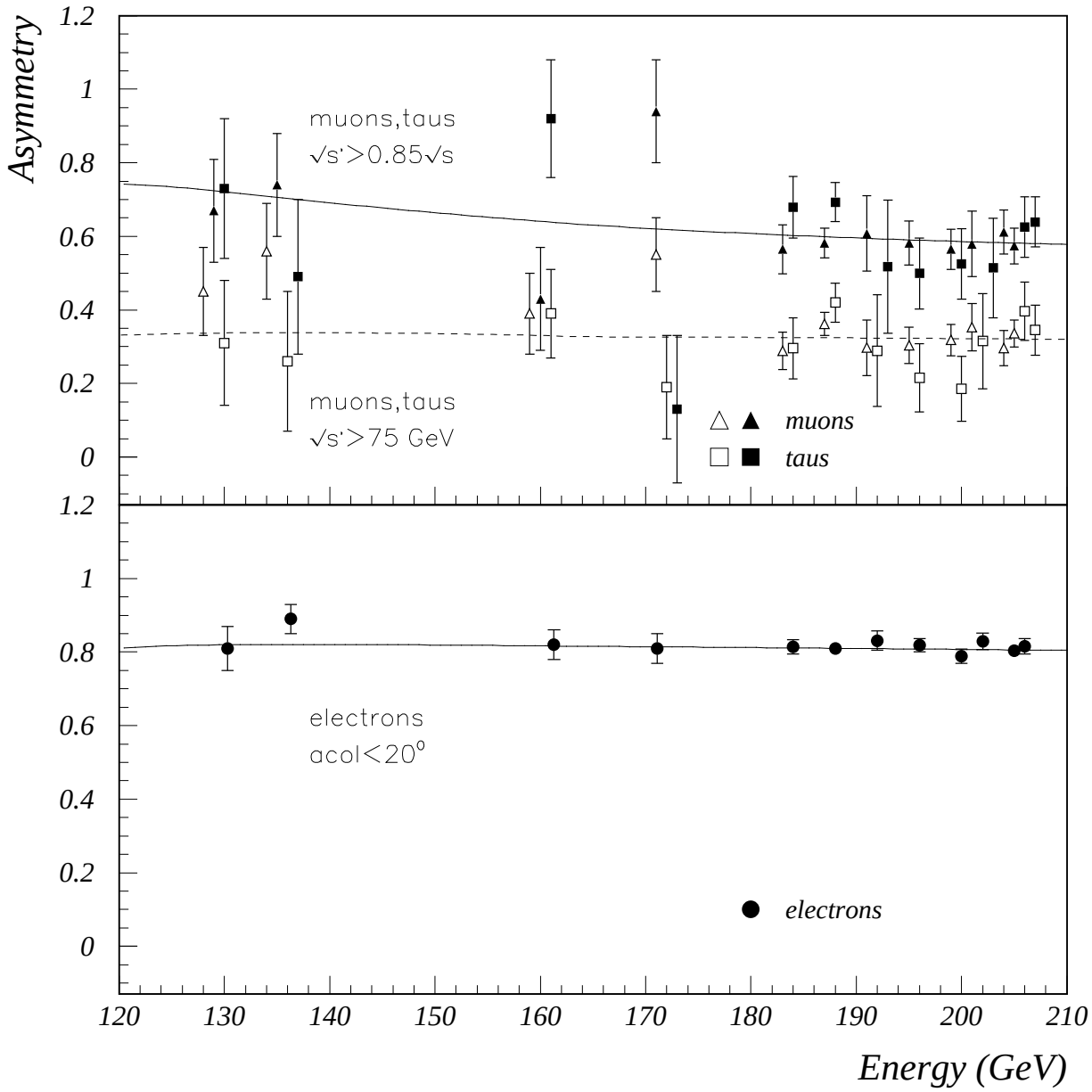

Figure 5: The forward-backward charge asymmetries in the reactions $e^+e^- \to \mu^+\mu^-(\gamma)$ and $\tau^+\tau^-(\gamma)$, and $e^+e^-(\gamma)$ measured at energies ranging from 130 to 206 GeV. The curves show the SM prediction of the TOPAZ0 program [15] for electron-positron final states and the ZFITTER program [14] for the other final states. Open points represent the *inclusive* selections and solid points the *non-radiative* selections.

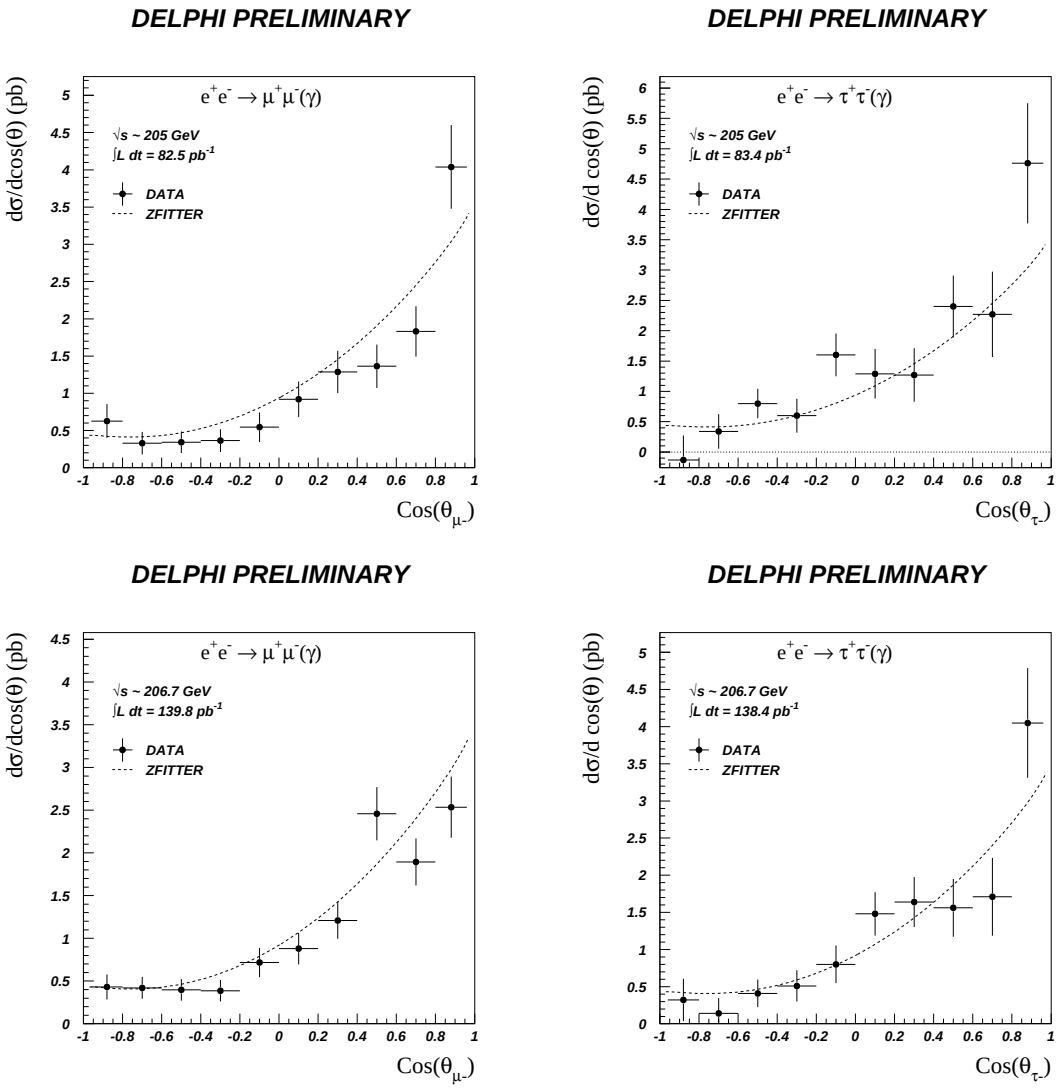

Figure 6: The weighted average of the differential cross-sections for measurements at $\sqrt{s} \sim 205 - 206\,\mathrm{GeV}$ for $\mu^+\mu^-$ and $\tau^+\tau^-$ final states. Also shown are the SM expectations calculated from ZFITTER for the differential cross-sections at the average value of $\sqrt{s}$.

$e^+e^- \to l^+l^-$			
Model	ϵ (TeV^{-2})	Λ^- (TeV)	Λ^+ (TeV)
LL	$-0.0061^{+0.0059}_{-0.0054}$	8.2	10.4
RR	$-0.0058^{+0.0058}_{-0.0065}$	7.8	9.9
VV	$-0.0050^{+0.0035}_{-0.0003}$	13.4	17.8
AA	$0.0013^{+0.0045}_{-0.0016}$	14.2	10.8
RL	$-0.0112^{+0.0045}_{-0.0079}$	6.4	9.9
LR	$-0.0112^{+0.0045}_{-0.0079}$	6.4	9.9

Table 4: Fitted values of ϵ and 95% confidence lower limits on the scale, Λ, of contact interactions in the models discussed in the text for $e^+e^- \to l^+l^-$, a combination of $e^+e^- \to e^+e^-$, $e^+e^- \to \mu^+\mu^-$ and $e^+e^- \to \tau^+\tau^-$ final states in which lepton universality is assumed for the contact interactions.

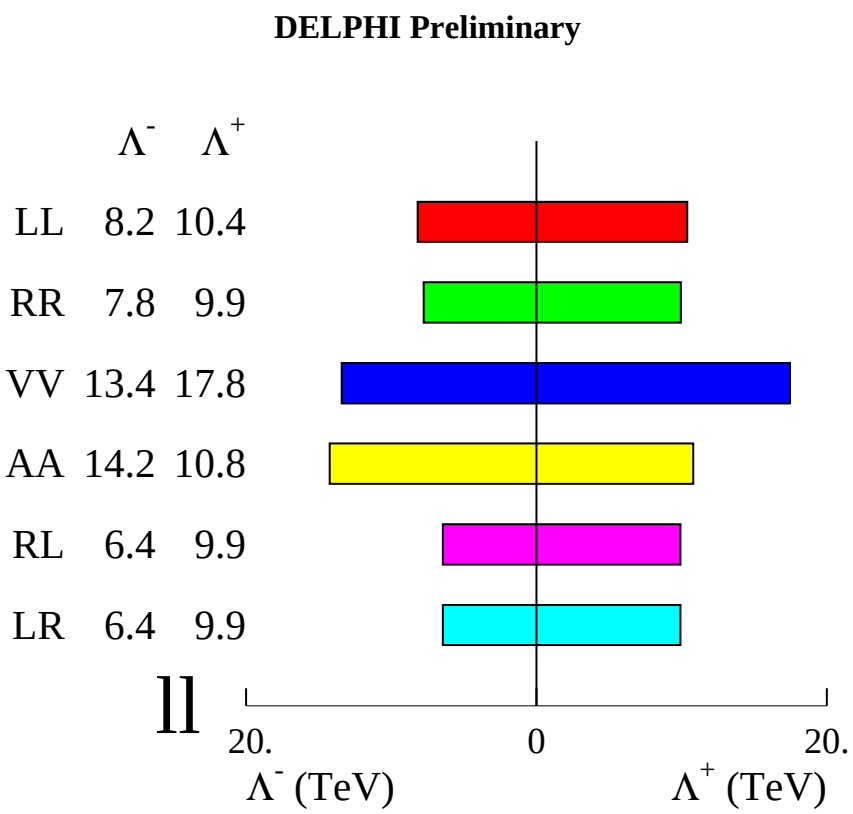

Figure 7: *The limits on* Λ *for* $e^+e^- \to l^+l^-$ *assuming universality in the contact interactions between* $e^+e^- \to e^+e^-, e^+e^- \to \mu^+\mu^-$ *and* $e^+e^- \to \tau^+\tau^-$.

Table 5, on the Z' mass range from approximately 336 to 503 GeV/c^2. The limits change by between 3 and 37 GeV/c^2 compared to the limits presented in [4], depending on the model.

For the Sequential Standard Model [20], which proposes the existence of a Z' with exactly the same coupling to fermions as the standard Z, a limit of $M_{Z'} > 656\,\mathrm{GeV}/c^2$ is found at 95% confidence. The change is -44 GeV/c^2 on the limit given in [4].

3.2.2 Model independent fits

Fits were performed to the leptonic cross-sections and forward-backward asymmetries, for the leptonic couplings of a Z', $a_{l'}^N$ and $v_{l'}^N$, normalised for the overall coupling scale and the mass of the Z' [19]. See section 5.4.2 and 6.3.2 of [2] for more details.

Several values of the mass of the Z' were considered (i.e. 300, 500 and 1000 GeV/c^2), and the ZZ'-mixing was neglected. The limits on the normalised couplings are $|a_{l'}^N| < 0.19$ and $|v_{l'}^N| < 0.21$, a change of 0.00 and -0.03, respectively, on limits given in [4].

4 Summary and conclusions

The results of the analyses of cross-sections and asymmetries above 200 GeV in the channels $e^+e^- \to e^+e^-(\gamma)$, $e^+e^- \to \mu^+\mu^-(\gamma)$, $e^+e^- \to \tau^+\tau^-(\gamma)$ and inclusive $e^+e^- \to q\bar{q}(\gamma)$, have been presented.

Overall, the data agree with the Standard Model predictions of ZFITTER and TOPAZ0. The data were used to update the searches for physics beyond the Standard Model given in [2, 3, 4]. No evidence for physics beyond the Standard Model was found, and limits were set on parameters of several more general models. The scale Λ characterising contact interactions between all leptons can be excluded at 95% confidence level in the range $\Lambda < 6.4 - 17.8$ TeV, depending on the model. Alternatively, Z' bosons lighter than $\sim 330\,\mathrm{GeV}/c^2$ can be excluded at the 95% confidence level in the models considered.

Acknowledgements

We thank the SL Division of CERN for the excellent performance of the LEP collider and our funding agencies.

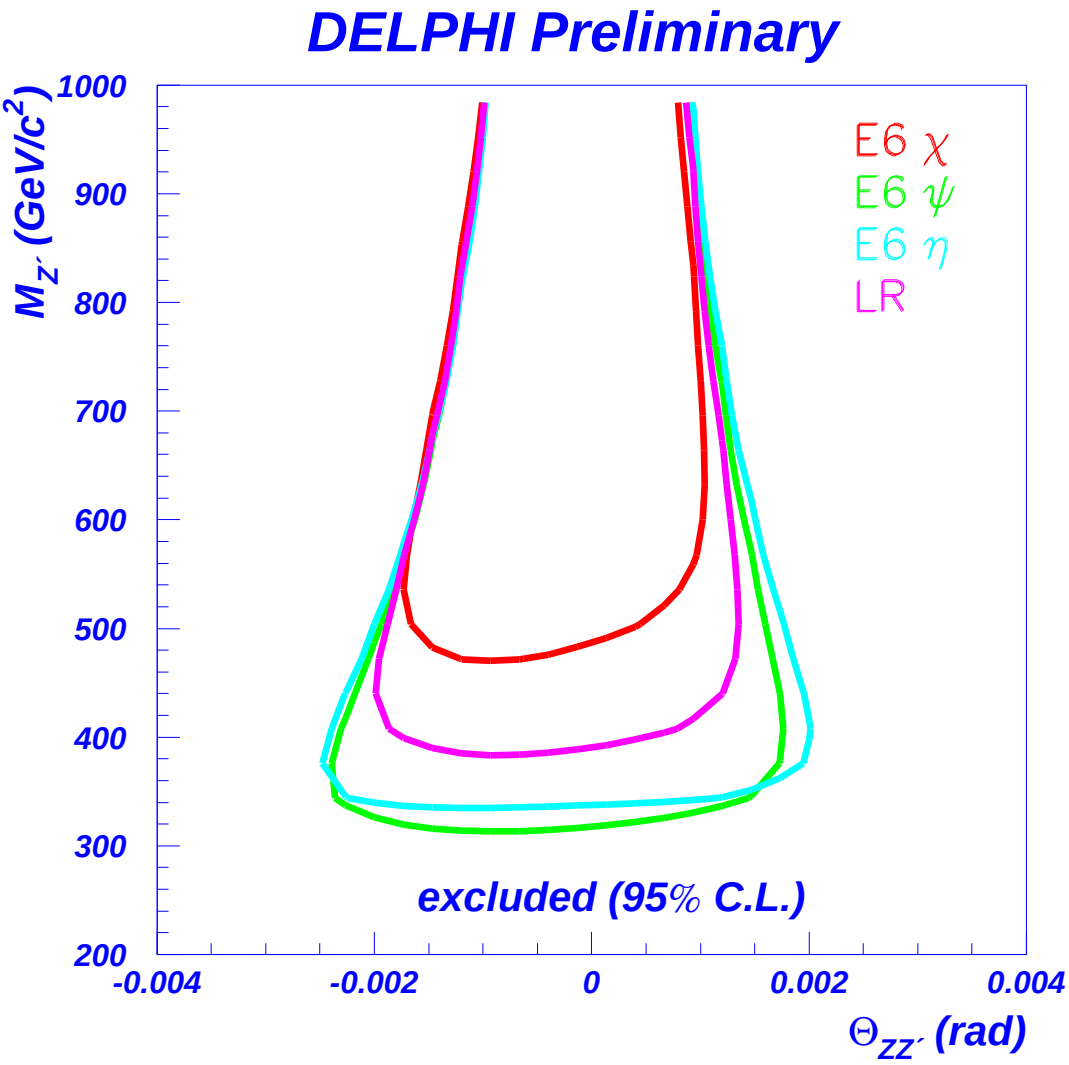

Figure 8: The allowed domain in the $M_{Z'} - \Theta_{ZZ'}$ plane for the χ, ψ, η and L-R models. The contours show the 95% confidence level limits.

Model	χ	ψ	η	L-R
$M_{Z'}^{limit}$ (GeV/c^2)	503	336	353	412
$\mid \Theta_{ZZ'}^{limit} \mid$ (mrad)	1.5	2.0	2.1	1.7

Table 5: 95% confidence level lower limits on the Z$'$ mass and upper limits on the ZZ$'$ mixing angle within the χ, ψ, η and L-R models.

References

[1] DELPHI Collaboration, P. Aarnio *et al.* , Nucl. Instr. & Meth. **A303** (1991) 233;
DELPHI Collaboration, P. Abreu *et al.* , Nucl. Instr. & Meth. **A378** (1996) 57.

[2] DELPHI Collaboration, P. Abreu *et al.* , Eur.Phys.J. **C11** (1999) 383.

[3] DELPHI Collaboration, P. Abreu *et al.* , Phys.Lett. **B485** (2000) 45.

[4] DELPHI Collaboration, Contributed Paper 647 to ICHEP (Osaka, July 2000), DELPHI 2000-128 CONF 427.

[5] DELPHI Collaboration, P. Abreu *et al.* , Nucl. Phys. **B417** (1994) 3.

[6] DELPHI Collaboration, P. Abreu *et al.* , Nucl. Phys. **B418** (1994) 403;
DELPHI Collaboration, P. Abreu *et al.* , Eur. Phys. J. **C16** (2000) 371.

[7] ALEPH Collaboration, D. Buskulic *et al.* , Phys. Lett. **B378** (1996) 373;
ALEPH Collaboration, R. Barate *et al.* , Phys. Lett. **B399** (1997) 329;
ALEPH Collaboration, R. Barate *et al.* , Euro. Phys. J. **C12** (2000) 183;
L3 Collaboration, M. Acciarri *et al.* , Phys. Lett. **B370** (1996) 195;
L3 Collaboration, M. Acciarri *et al.* , Phys. Lett. **B407** (1997) 361;
L3 Collaboration, M. Acciarri *et al.* , Phys. Lett. **B433** (1998) 163;
L3 Collaboration, M. Acciarri *et al.* , Phys. Lett. **B464** (1999) 135;
L3 Collaboration, M. Acciarri *et al.* , Phys. Lett. **B470** (1999) 281;
L3 Collaboration, M. Acciarri *et al.* , Phys. Lett. **B479** (2000) 101;
L3 Collaboration, M. Acciarri *et al.* , Phys. Lett. **B489** (2000) 81;
OPAL Collaboration, G. Alexander *et al.* , Phys. Lett. **B387** (1996) 432;
OPAL Collaboration, K. Ackerstaff *et al.* , Phys. Lett. **B391** (1997) 221;
OPAL Collaboration, K. Ackerstaff *et al.* , Euro. Phys. J. **C2** (1998) 441;
OPAL Collaboration, G. Abbiendi *et al.* , Euro. Phys. J. **C6** (1999) 1;
OPAL Collaboration, G. Abbiendi *et al.* , Euro. Phys. J. **C13** (2000) 553;

[8] LEP Energy Working Group 99-01;
CERN-EP/98-191

[9] T. Sjöstrand, PYTHIA 5.7/JETSET 7.4 CERN-TH 7112/93 (1993).

[10] F. A. Berends, R. Pittau and R. Kliess, Comp. Phys. Comm. **85** (1995) 437.

[11] S. Nova *et al.* , DELPHI Note 90-35.

[12] F. A. Berends, P. H. Daverveldt and R. Klies, Comp. Phys. Comm. **40** (1986) 271.

[13] S. Jadach, B.F.L. Ward and Z. Was, Comp. Phys. Comm. **79** (1994) 503.

[14] D. Bardin *et al.* , *"ZFITTER: An Analytical Program for Fermion Pair Production in e^+e^- Annihilation"*, HEP-PH/9908433 (1999).

[15] G. Montagna *et al.* , Nucl. Phys. **B401** (1993) 3;
G. Montagna *et al.* , Comput. Phys. Commun. **76** (1993) 328.

[16] E. Eichten, K. Lane and M. Peskin, Phys. Rev. Lett. **50** (1983) 811.

[17] P. Langacker, R.W. Robinett and J.L. Rosner, Phys. Rev. **D30** (1984) 1470;
D. London and J.L. Rosner, Phys. Rev. **D34** (1986) 1530;
J.C. Pati and A. Salam, Phys. Rev. **D10** (1974) 275;
R.N. Mohapatra and J.C. Pati, Phys. Rev. **D11** (1975) 566.

[18] F. James, *"MINUIT Reference Manual"*, CERN Program Library Long Writeup D506 (1994).

[19] A. Leike, Zeit. Phys. **C62** (1994) 265.

[20] G. Altarelli *et al.* , Z. Phys. C45 (1989) 109;
erratum Z. Phys. C47 (1990) 676.